Article

Molybdenum Oxide-Modified Iridium Catalysts for Selective Production of Renewable Oils for Jet and Diesel Fuels and Lubricants

Sibao Liu, Weiqing Zheng, Jiayi Fu, Konstantinos Alexopoulos, Basudeb Saha, and Dionisios G. Vlachos

Just Accepted

Molybdenum Oxide-Modified Iridium Catalysts for Selective Production of Renewable Oils for Jet and Diesel Fuels and Lubricants

Sibao Liu,[1] Weiqing Zheng,[1] Jiayi Fu[1,2], Konstantinos Alexopoulos[1,2], Basudeb Saha,[1]* and Dionisios G. Vlachos[1,2]*

[1]Catalysis Center for Energy Innovation, University of Delaware, Newark, DE 19716, USA

[2]Department of Chemical and Biomolecular Engineering, University of Delaware, Newark, DE 19716, USA

*Corresponding authors: vlachos@udel.edu, bsaha@udel.edu

Abstract

Supported inverse metal-metal oxide catalysts have received significant research interest owing to their effective hydrodeoxygenation (HDO) activity toward biomass substrates but the high cost of the reported catalysts poses a challenge for commercialization. We present the synthesis of a series of metal-metal oxide catalysts, Ir-MO$_x$/SiO$_2$ (M=Re, Mo, W, V, or Nb) and M'-MoO$_x$/SiO$_2$ (M=Rh, Ru, Pt, or Pd), and their HDO performance on multi-furan (high carbon) substrates to produce renewable jet and diesel fuels and lubricants base oils. A MoO$_x$ modified Ir/SiO$_2$ catalyst with Mo/Ir ratio of 0.13 (Ir-MoO$_x$/SiO$_2$) exhibits the highest product yield (78-96%) under mild reaction conditions. Controlled experiments using probe substrates reveal that furan ring hydrogenation and C−O hydrogenolysis of saturated and unsaturated furan rings occur in a sequential manner. The carbon atom adjacent to the furan or saturated furan ring of substrates or intermediate compounds undergoes slow C−C bond scission resulting in a small fraction of lighter alkanes. Catalyst characterization suggests that Ir is reduced to fully metallic state to dissociate hydrogen for hydrogenation. Intact MoO$_x$, partly covering the Ir metal surface, promotes ring opening, hydrogenolysis of etheric and alcoholic C−O bonds, and hydrogenation of C=O bonds. This study highlights the potential of low-cost metal-metal oxide catalysts with low loading of oxophilic metals to enable cost-competitive production of bioproducts and demonstrates applicability of these catalysts on other substrates, including fatty acids, fatty esters, and lipids.

1

2

1. Introduction

Global carbon emissions drive exploration of lignocellulosic biomass as a renewable resource for chemicals and fuels[1-7]. Long-chain alkanes, with varying carbon number and structure (linear or branched), used for jet fuel (C_8-C_{16}), diesel fuel (C_9-C_{22}), and lubricant base oils (C_{20}-C_{50}), collectively called oils, are conventionally produced from petroleum. Branched alkanes are preferred oils for their improved cold flow properties[8]. Production of high-volume oils from abundant, inexpensive, and carbon-neutral lignocellulose could mitigate carbon emission challenges.

While the synthesis of fuels from furan platforms (e.g., furfural, 2-methylfuran) has been reported[9-25], the synthesis of lubricant base oils is still in its infancy[26-29]. High carbon alkanes can be synthesized by carbon-carbon (C−C) coupling of furans with bio-based carbonyl compounds to obtain high carbon furans (HCFs) followed by their hydrodeoxygenation (HDO) to alkanes. C−C coupling reactions, e.g., hydroxyalkylation/alkylation[9-15, 17, 30], conjugate addition/ hydroxyalkylation/alkylation[31], aldol condensation[20, 22-23], alkylation[18], benzoin condensation[21, 25], can achieve high yields using acid or base catalysts. HDO, on the other hand, requires high reaction temperatures and pressures[14, 24] that lead to high utility and energy costs and undesirable C−C cracking[14-15]. We recently reported a supported inverse metal-metal oxide catalyst, partially reduced rhenium oxide modified Ir/SiO$_2$ catalyst (Ir-ReO$_x$/SiO$_2$), is efficient for the HDO of C_{12}-C_{34} HCFs to produce high yield, long-chain branched alkanes under mild reaction conditions[16, 29, 31]. Replacement of the expensive Re (~7.8 wt%, \$1290/lb)[32] with a low-cost metal-inexpensive oxophilic metal oxide (e.g., molybdenum, \$12.6/lb)[33] will be preferable.

Prior reports suggest that several non-noble oxophilic metal oxides, including MoO$_x$, WO$_x$, VO$_x$, or NbO$_x$ modified with noble metal are selective for hydrogenation and hydrogenolysis reactions[34], including the ring opening of cyclic ethers with -OH groups to diols[35-40], the hydrogenolysis of polyols to mono-alcohols[41-42], the hydrogenation of unsaturated aldehydes to unsaturated alcohols[43-44], and the hydrogenation of amino acids to amino alcohols[45-46]. The noble metal and the partially reduced metal oxide cooperate toward enhanced activity and selectivity[34]. Some of them, e.g., NbO$_x$, perform even better than ReO$_x$ in the selective hydrogenation of unsaturated aldehydes[44]. Despite these efforts, complete HDO of furan compounds to alkanes over such inexpensive catalysts has not been reported.

3

In this work, cheap oxophilic metal oxides (MoO_x, WO_x, VO_x, and NbO_x) modified Ir/SiO_2 catalysts ($Ir-MoO_x/SiO_2$, $Ir-WO_x/SiO_2$, $Ir-VO_x/SiO_2$, and $Ir-NbO_x/SiO_2$) are synthesized and tested for HDO of HCFs to produce renewable oils under mild reaction conditions (Scheme 1). Among them, $Ir-MoO_x/SiO_2$ (Mo/Ir=0.13) catalyst exhibits superior performance (up to 96% yield) than our previously reported $Ir-ReO_x/SiO_2$ with the same low metal loading. Control reactions, using probe molecules, and catalyst characterization are conducted to elucidate the reaction pathway and the promoting effect of MoO_x.

4

A)

B)

Scheme 1. A): Production of jet and diesel fuels (C_{15}-A and C_{14}-A) from 2-methylfuran with different carbonyl compounds (C_{15}-HCF1, C_{14}-HCF and C_{15}-HCF2) and their subsequent HDO over Ir-MoO$_x$/SiO$_2$. B): Production of lubricant base oils (C_{20}-A and C_{30}-A) from 2-pentylfuran and different aldehydes (C_{20}-HCF and C_{30}-HCF) and their subsequent HDO over Ir-MoO$_x$/SiO$_2$.

5

2. Experimental

2.1. Catalyst preparation

Ir-MO$_x$/SiO$_2$ (M=Re, Mo, W, V or Nb) catalysts were prepared by sequential impregnation as described previously[16, 29]. First, Ir/SiO$_2$ was prepared by impregnating SiO$_2$ (Fuji Silysia G-6, calcined in air at 700 °C for 1 h with a heating rate of 10 °C/min, and BET surface area 535 m^2/g) with an aqueous solution of H$_2$IrCl$_6$ (Sigma-Aldrich). After evaporating the solvent at 75 °C and drying at 110 °C for 12 h, impregnation happened with an aqueous solution of either NH$_4$ReO$_4$ (Alfa-Aesar), (NH$_4$)$_6$Mo$_7$O$_{24}$·4H$_2$O (Alfa-Aesar), (NH$_4$)$_{10}$W$_{12}$O$_{24}$·5H$_2$O (Sigma-Aldrich), NH$_4$VO$_3$ (Sigma-Aldrich), (NH$_4$)NbO(C$_2$O$_4$)$_2$·5H$_2$O (Sigma-Aldrich). Catalysts were dried at 110 °C for 12 h and then calcined in a crucible in air at 500 °C for 3 h by ramping at 10 °C/min. The loading of Ir was 4.0 wt% and the M/Ir atomic ratio ranged from 0 to 0.5. Other metal impregnated catalysts, M'-MoO$_x$/SiO$_2$ (M=Rh, Ru, Pt or Pd, Mo/M'=0.25), were prepared following the same procedure using RhCl$_3$ (Alfa-Aesar), RuCl$_3$ (Sigma-Aldrich), H$_2$PtCl$_6$ (Sigma-Aldrich), and PdCl$_2$ (Sigma-Aldrich). These catalysts are hereafter referred to as M'-MO$_x$/SiO$_2$.

2.2. Synthesis of high carbon furans (HCFs)

HCFs were prepared by HAA of 2-methylfuran (2-MF) or 2-pentylfuran with carbonyl compounds following our previous work[9, 29-30]. In brief, the HAA reaction was carried out in a round-bottom flask equipped with a reflux condenser and a magnetic stirrer. The reaction temperature was controlled using an oil bath. C$_{14}$- and C$_{15}$- HCFs (Scheme 1) were synthesized by the HAA reaction of 2-MF with furfural and butanal, respectively, over an improved graphene oxide catalyst[30]. C$_{15}$-HCF2 was synthesized by self-condensation of 2-MF over H$_2$SO$_4$.[9] C$_{20}$-HCF and C$_{30}$-HCF were prepared by reacting 2-pentylfuran with acetaldehyde and lauraldehyde, respectively, over a perfluorinated sulfonic acid resin (Aquivion PW98) catalyst[29].

2.3. Hydrogenation of C$_{15}$-HCF1

Hydrogenation of the furan rings of C$_{15}$-HCF1 was conducted in a 50-ml Parr reactor with an inserted Teflon liner over a Pd/C (10 wt% Pd, Sigma-Aldrich) catalyst. C$_{15}$-HCF1 (1 g), Pd/C (0.1 g) and solvent (cyclohexane;10 mL) were added into the Teflon liner together with a magnetic stirrer. The liner was then placed in the reactor, which was heated at 60 °C with 6 MPa H$_2$ for 4 h. After reaction, the catalyst was separated by centrifugation. The product was obtained after removing the solvent by a rotary evaporator.

6

2.4. HDO of HCFs over metal-metal oxide catalysts

HDO reaction was performed in a 50-ml Parr reactor with an inserted Teflon liner. The catalyst was placed into the Teflon liner together with a magnetic stirrer and 10 ml solvent (cyclohexane). The reactor, equipped with a band heater, was heated at 200 °C with 5 MPa H_2 for 1 h to reduce the catalyst. The stirrer speed was set at 240 rpm. After pre-reduction, the reactor was cooled down, and the pressure released. The reactor was immediately loaded with 0.3 g HCF substrates or hydrogenated C_{15}-HCF1 product and sealed. The sealed reactor was purged with H_2 (1 MPa) for three times and pressurized to 5 MPa with H_2 and then heated to reaction temperature. The total time to reach the set temperature was about 25 min. The stirring rate was set at 500 rpm. After a certain reaction time, the reactor was placed in an ice-water bath and upon cooling, the pressure released. The reaction solution, along with the spent catalyst, were transferred to a glass vial. The spent catalyst was separated by centrifugation and filtration. In the catalyst recyclability tests, the used catalyst after each cycle was washed three times with 10 ml cyclohexane, dried at 110 °C for 12 h, and then regenerated by calcination at 400 °C for 3 h at a heating rate of 10 °C/min.

The HDO reactions of 2,5-dimethylfuran (DMF, Sigma Aldrich), 2,5-dimethyltetrahydrofuran (DMTHF, Sigma Aldrich), 2-hexanone (TCI America) and 2-hexanol (Sigma Aldrich) were performed in the similar way. DMF was distilled to remove any impurities before reaction. To avoid the hydrogenation reaction of furan rings during heating, the reactor was first pressurized with 0.3 MPa N_2 during heating to the set temperature and then pressurized with H_2 to a total pressure of 6 MPa. Control experiments suggested no conversion of the substrate until the introduction of hydrogen.

Product analysis was done with a gas chromatograph, GC (Agilent 7890A), equipped with an HP-1 column and a flame ionization detector using icosane (C_{20}) as an internal standard. DMF, DMTHF, 2-hexanone, and 2-hexanol hydrotreated products were analysed with a GC (Agilent 7890B) equipped with an HP-INNOWax column and a flame ionization detector using *n*-decane as an internal standard. Since a small fraction of cyclohexane (solvent) could be cracked to linear alkanes during the catalyst pre-reduction and reaction over some of the catalysts, any detected C_1-C_6 alkanes in the gas or liquid phase, that could form during HDO of HCFs, were not quantified. The products from HDO of C_{15}-HCF1 were also analyzed using a Nicolet 8700 FTIR spectrometer equipped with a DTG detector and a Golden Gate single reflection diamond attenuated total

7

reflectance (ATR) attachment. All FTIR spectra were acquired at 32 scans with a resolution of 2 cm^{-1}.

The conversion of furans and the yield of products were calculated on carbon basis and defined as follows:

$$\text{Conversion [\%]} = \frac{\text{mole of initial reactant} - \text{mole of unreacted reactant}}{\text{mole of initial reactant}} \times 100$$

$$\text{Yield of detected products [\% - C]} = \frac{\text{mol}^{\text{product}} \times \text{C atoms in product}}{\text{mol of total C atoms of initial reactant}} \times 100$$

2.5. Characterization of Ir-MoO$_x$/SiO$_2$

X-ray diffractograms (XRD) of the pre-reduced and recovered catalysts were recorded by a diffractometer (Bruker D8) equipped with a Cu Kα radiation source (λ=0.154nm) at 40 kV and 40 mA. X-ray photoelectron spectroscopy (XPS) experiments were conducted using a Thermo-Fisher K-alpha+X-ray photoelectron spectrometer equipped with a monochromatic aluminum K-alpha X-ray source (400 μm). Before analysis, the Ir-MoO$_x$/SiO$_2$ catalyst was pre-reduced as detailed above and then transferred into the K-Alpha$^+$ Vacuum Transfer Module (VTM, ThermoScientific) without being exposed to air.

X-ray absorption spectroscopy (XAS) data were collected for the Mo K edge (20000 eV) at the bending magnet beamline (5BM-D) of the Dow-Northwestern-DuPont Collaborative Access Team (DND-CAT) of the Advanced Photon Source, Argonne National Laboratory. The measurements for reference samples (Na$_2$MoO$_4$, MoO$_3$, MoO$_2$ and Mo foil) were taken in transmission mode. The samples were pelletized using a die of diameter 13mm and then held in a cell (Linkam stage). The Ir-MoO$_x$/SiO$_2$ and MoO$_x$/SiO$_2$ were in-situ recorded in fluorescence mode. The catalysts were reduced in flowing N$_2$ (90 ml/min) and H$_2$ (10 ml/min) at 200 °C for 1h by ramping at 10 °C/min. Spectra were recorded before and after reduction.

The FTIR spectra of pyridine adsorbed on MoO$_x$/SiO$_2$ and Ir-MoO$_x$/SiO$_2$ were collected on a Thermo Electron Nicolte 8700 FT-IR Spectrometer equipped with an MCT detector (128 scans at a spectral resolution of 2 cm^{-1}) and an in-house made *in situ* transmission cell. The transmission cell was held at a vacuum level of 0.01 mTorr through a vacuum manifold, which is connected to a mechanical pump and a diffusion pump. A self-standing catalyst wafer was loaded into a custom-made sample holder and the catalyst was reduced at 200 °C under a hydrogen stream (20 ml/min)

8

for 1 h. Upon cooling to room temperature and evacuation, 100 mTorr of pyridine was introduced to the transmission cell via the vacuum manifold, and IR spectra were collected at 150 °C.

The microstructures of the catalysts after pre-reduction were examined using a field emission transmission electron microscope JEM-2010F FasTEM at 200 kV.

Quantification of leaching from Ir-MoO$_x$/SiO$_2$ in the product solutions was conducted using a triple quadrupole inductively coupled plasma mass spectrometer (Thermo Scientific iCAP TQ-ICP-MS).

3. Results and discussion

3.1 Catalysts screening and reaction conditions optimization

First, the catalyst performance was screened for HDO of C$_{15}$-HCF1 (Scheme 1) over Ir-MO$_x$/SiO$_2$ catalysts. The first set of experiments used catalysts containing Ir as the metal sites and various inexpensive oxophilic metals such as MoO$_x$, WO$_x$, VO$_x$ and NbO$_x$ as oxides. The Ir loading was the same as in our previously reported Ir-ReO$_x$/SiO$_2$ whereas the atomic ratio of M/Ir was lower (0.25) (Re/Ir ratio in Ir-ReO$_x$/SiO$_2$ was 2)[16]. This is significant to preserve metals and reduce catalysts preparation costs. Ir-ReO$_x$/SiO$_2$ catalyst with Re/Ir atomic ratio of 0.25 was also synthesized for comparison. Table 1 shows that Ir/SiO$_2$ without any oxophilic metal oxide exhibits very low activity (Entry 1)[16]. In contrast, Ir-MO$_x$/SiO$_2$ enhances the HDO activity significantly (Table 1, Entries 2-4 and 6). The Ir-MoO$_x$/SiO$_2$ (0.25) catalyst exhibits the highest yield to branched alkanes (Table 1, Entry 2). Ir-ReO$_x$/SiO$_2$ (0.25), Ir-WO$_x$/SiO$_2$ (0.25), and Ir-VO$_x$/SiO$_2$ (0.25) show a moderate catalytic performance and a significant fraction of unconverted oxygenated species. Ir-NbO$_x$/SiO$_2$ (0.25) is inefficient (Table 1, Entry 5). This result for Ir-NbO$_x$/SiO$_2$ differs from prior reports in which noble metals (Pd and Pt) supported on Nb-based materials (NbOPO$_4$, Nb$_2$O$_5$, and Nb$_2$O$_5$/SiO$_2$) were used for HDO of single and multi-ring furan substrates.[17, 22, 28, 47-51] This difference in catalytic performance is probably due to the difference in catalysts' structures and compositions. Among the M'-MoO$_x$/SiO$_2$ (0.25) catalysts, Rh-MoO$_x$/SiO$_2$ and Pt-MoO$_x$/SiO$_2$ yield only 12-14% long chain alkanes (Table 1, Entries 7 and 8). Ru-MoO$_x$/SiO$_2$ (0.25) and Pd-MoO$_x$/SiO$_2$ (0.25) yields primarily unconverted oxygenated intermediates (Table 1, Entries 9 and 10). The latter series of catalysts with other hydrogenation metals perform worse than Ir-MoO$_x$/SiO$_2$ (0.25).

9

Table 1. HDO of C_{15}-HCF1 over M'-MO_x/SiO_2 catalysts.

Entry	Catalyst	M/M'	Conv. %	Yield %									Oxygenates
				C_8	C_9	C_{10}	C_{11}	C_{12}	C_{13}	C_{14}	C_{15}	Sum	
1	Ir/SiO_2	0	99	0.0	0.0	0.8	0.9	0.2	0.6	0.1	3.3	6	47
2	Ir-MoO_x/SiO_2	0.25	100	0.0	0.1	14	19	0.1	0.1	0.6	43	77	2.0
3	Ir-WO_x/SiO_2	0.25	100	0.0	0.1	7.8	14	2.9	0.1	0.3	19	44	30
4	Ir-VO_x/SiO_2	0.25	100	0.1	0.3	14	22	2.3	0.1	0.3	10	50	16
5	Ir-NbO_x/SiO_2	0.25	100	0.1	0.0	0.4	0.4	0.0	0.0	0.0	0.3	1.3	54
6	Ir-ReO_x/SiO_2	0.25	100	0.0	0.2	9.3	14	1.3	0.1	0.5	27	52	21
7	Rh-MoO_x/SiO_2	0.25	100	0.0	0.2	3.1	2.8	0.0	0.0	0.1	7.5	14	55
8	Pt-MoO_x/SiO_2	0.25	100	0.0	0.1	6.3	3.0	0.2	0.0	0.1	2.5	12	74
9	Ru-MoO_x/SiO_2	0.25	100	0.0	0.1	0.2	0.2	0.0	0.0	0.1	0.2	0.9	72
10	Pd-MoO_x/SiO_2	0.25	100	0.0	0.0	0.1	0.1	0.0	0.0	0.0	0.4	0.0	60
11	Ir-MoO_x/SiO_2	0.05	100	0.0	0.1	12	17	0.1	0.1	0.5	41	71	3.5
12	Ir-MoO_x/SiO_2	0.13	100	0.0	0.1	13	21	0.1	0.2	0.7	43	78	0.0
13	Ir-MoO_x/SiO_2	0.5	100	0.0	0.2	13	16	0.1	0.1	0.6	39	69	1.8
14	MoO_x/SiO_2	-	34	0.0	0.0	0.0	0.0	0.0	0.0	0.0	0.0	0.0	4.0
15[a]	Ir/SiO_2 +MoO_x/SiO_2	-	100	0.0	0.1	8.2	18	0.3	0.1	0.2	13	40	29

Reaction conditions: catalyst (0.15 g), M': Ir, Rh, Pt, Ru, Pd (4 wt%), M: Mo, W, V, Nb, Re, C_{15}-HCF1 (0.3 g), cyclohexane (10 mL), initial H_2 (5 MPa), 180 °C, 20 h. a: physical mixture of Ir/SiO_2 and MoO_x/SiO_2 with the same metal amount of Ir-MoO_x/SiO_2 (0.13).

10

Next, Ir-MoO$_x$/SiO$_2$ catalysts of Mo/Ir atomic ratio varying between 0.05 to 0.5 were screened. These catalysts achieve full conversion of C$_{15}$-HCF1. The yield to long chain alkanes and the desired C$_{15}$ alkane (hereinafter referred to as C$_{15}$-A, Scheme 1) shows a volcano-type behavior vs. the atomic ratio of Mo/Ir (Table 1, Entries 2 and 11-13) with the Ir-MoO$_x$/SiO$_2$ (0.13) giving the highest conversion and total yield of C$_8$-C$_{15}$ alkanes (78%) (Table 1, Entry 12). Control experiments over either Ir/SiO$_2$ or MoO$_x$/SiO$_2$ exhibit no reaction (Table 1, Entries 1 and 14). A physical mixture of Ir/SiO$_2$ and MoO$_x$/SiO$_2$ at Mo/Ir=0.13 yields 29% C$_8$-C$_{15}$ alkanes (Table1, Entry 15), indicating a synergy. Since Ir-MoO$_x$/SiO$_2$ (0.13) achieves the best performance, it was chosen for all subsequent experiments.

The effects of reaction temperature and initial hydrogen pressure on the Ir-MoO$_x$/SiO$_2$ are shown in Tables S1 and S2. The conversion of C$_{15}$-HCF1 and the yield to total alkanes, with C$_{15}$-A being the major product, increases remarkably with increasing reaction temperature from 160 °C to 170 °C. Higher temperature ($\geq$190 °C) cause a slight decrease in the yield of total alkanes as well as of C$_{15}$-A, with a concurrent increase in the yield of C$_{10}$ and C$_{11}$ alkanes *via* C−C cleavage. Increasing H$_2$ pressure from 2 to 5 MPa exhibits no effect on C15-HCF1 conversion but an enhanced selectivity to C$_{15}$-A (Table S2) due to less C−C cracking. Since C−C cleavage mainly occurs at the tertiary carbon center adjacent to furan moieties[9, 14, 16], higher H$_2$ pressure favors hydrogenation of furan rings and HDO of saturated of furan rings. Further increase in H$_2$ pressure to 6 MPa shows no pronounced effect on the reaction. Therefore, 180 °C and 5 MPa H$_2$ pressure were chosen for the time course investigation discussed below.

3.2 Time dependent studies and reaction network

To understand the reaction network for HDO of multi-furan substrates, the time course of C$_{15}$-HCF1 was investigated using the Ir-MoO$_x$/SiO$_2$ (0.13) catalyst (Figure 1). The majority of C$_{15}$-HCF1 is converted during heating, and conversion is nearly quantitative within 2 h. First, oxygenated intermediates form as major products by hydrogenation of furan rings. These oxygenates are then deoxygenated into alkanes. GC-MS and ATR-IR analysis reveals that the oxygenated intermediates at the beginning of the reaction consist mainly of saturated furan ring, mono-keto and mono-hydroxyl groups (Figure S1 and S2). Similar functional groups were also observed over the Ir-ReO$_x$/SiO$_2$ (2) in our earlier work[16]. Complete deoxygenation of all oxygenated intermediates to alkanes occurs within 20 h. No C−C cleavage of long chain alkanes is evidenced when continuing the reaction for a longer time, indicating that Ir-MoO$_x$/SiO$_2$ does not

11

catalyze C−C cracking of alkanes after they form; rather, C−C cleavage of C_{15} oxygenates occurs during deoxygenation. The highest yield of total alkanes reaches 78% with 43% of it being branched C_{15}-A.
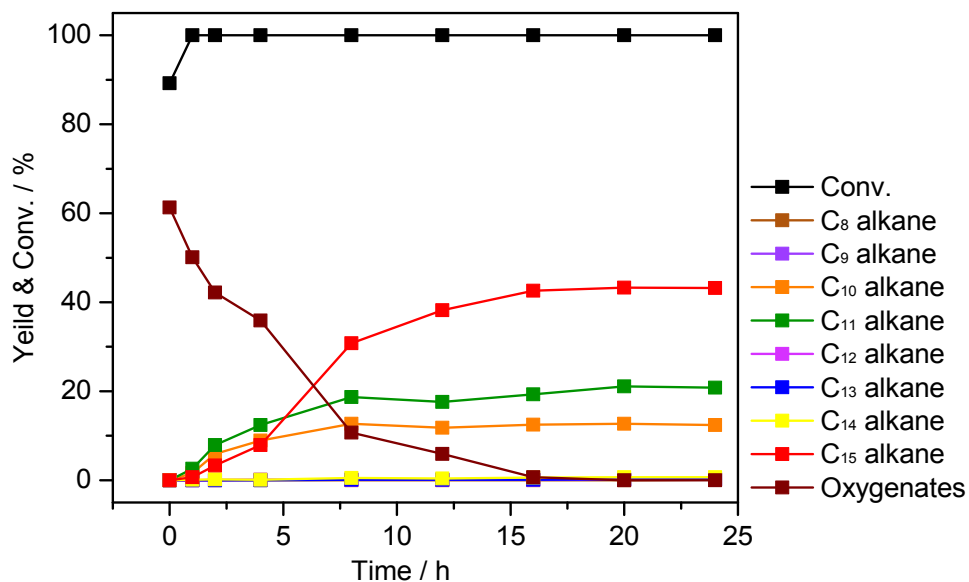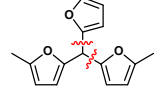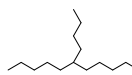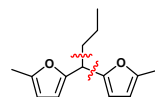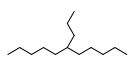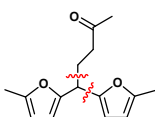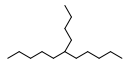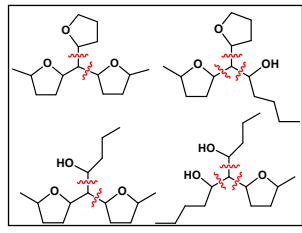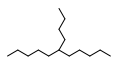

Figure 1. Reaction profile of C_{15}-CF1 HDO over the Ir-MoO$_x$/SiO$_2$ (0.13) catalyst. Reaction conditions: catalyst (0.15 g), C_{15}-CF1 (0.3 g), cyclohexane (10 mL), initial H_2 (5 MPa), and 180 ℃.

Two other main alkanes, *n*-decane (13%) and *n*-undecane (21%), result from the C−C bond scission adjacent to the tertiary carbon atom. C−C cleavage leads to a C_5 or C_4 moiety, which likely deoxygenates to pentane or butane present in the gas phase. Important intermediates detected include 2-methyl-5-pentyltetrahydrofuran, 2-hexyl-5-methyltetrahydrofuran, 5-decanol, 2-undecanol and 5-undecanol (Figure S3). These oxygenates were converted to *n*-decane and *n*-undecane during progression of the reaction.

Table 2. HDO of different oxygenated precursors over Ir-MoO$_x$/SiO$_2$ (0.13) catalyst.

			Yield %		
Entry	Substrate	Conv. %	Desired alkane	C-C cracked alkanes	Sum of fuel-ranged alkanes

12

1	C$_{15}$-HCF1	100	43	C$_{10}$ 12.4 C$_{11}$ 20.8	78
2	C$_{14}$-HCF	100	86	C$_{9}$ 7.7 C$_{11}$ 0.4	95
3	C$_{15}$-HCF2	100	85	C$_{10}$ 3.8 C$_{11}$ 0.2	89
4	Hydrogenated C$_{15}$-HCF1	100	88	C$_{10}$ 3.6 C$_{11}$ 3.5	96

Reaction conditions: catalyst (0.15 g), substrate (0.3 g), cyclohexane (10 mL), initial H$_2$ (5 MPa), 180 °C, 24 h.

To understand the C−C cleavage pathways, model compounds of high carbon furan with alkyl chain (C$_{14}$-HCF) and mono-keto chain (C$_{15}$-HCF2) and hydrogenated C$_{15}$-HCF1 with saturated furan rings were exploited (Table 2). HDO of C$_{14}$-HCF and C$_{15}$-HCF2 results in no C−C scission between the tertiary carbon center and the alkyl or mono-keto moiety (Table 2, Entries 2 and 3). C−C scission of both compounds occurs between the furan moiety and the tertiary carbon atom (Table 2, Entries 2 and 3). HDO of hydrogenated furan rings of C$_{15}$-HCF1 yields C$_{10}$ and C$_{11}$ alkanes, but their yields are significantly lower than those from the HDO of C$_{15}$-HCF1 (Table 2, Entries 1 and 4). This finding indicates that C−C scission occurs at the carbon center adjacent to the furan rings and saturated furan rings during the hydrogenation/HDO steps. This finding differs from prior reports[9, 14] that hypothesized that C−C scission only occurs at the tertiary carbon center adjacent to the furans. One-step HDO of C$_{14}$-HCF achieves 95% fuel-ranged alkanes (Table 2, Entry 2). 96% yield of alkanes is obtained by hydrogenation at low temperature over Pd/C followed by HDO of hydrogenated C$_{15}$-HCF1 at high temperature over Ir-MoO$_x$/SiO$_2$ (0.13) (Table 2, Entry 4). These yields are comparable to those over Ir-ReO$_x$/SiO$_2$ (2)[16] and significantly higher than those over Ni/HBEA and Ni/HZSM-5 catalysts (~80%) reported in the literature[14-15]. Importantly,

13

our reaction temperature (180 ^{o}C) is lower than that used (230 ^{o}C) for Ni-based catalysts, underscoring the effectiveness of Ir-MoO$_x$/SiO$_2$ for HDO of high carbon furan compounds.

The overall reaction pathway for HDO of C$_{15}$-HCF1 is depicted in Scheme 2. The furan rings of C$_{15}$-HCF1 undergo ring saturation and ring opening in parallel to form a mixture of oxygenates with three different functional branches including saturated furan rings, carbonyl groups, and hydroxyl groups mainly during heating. The HDO of these oxygenates results in alkanes. C−C scission occurs at the carbon atom adjacent to the furan or saturated furan rings.
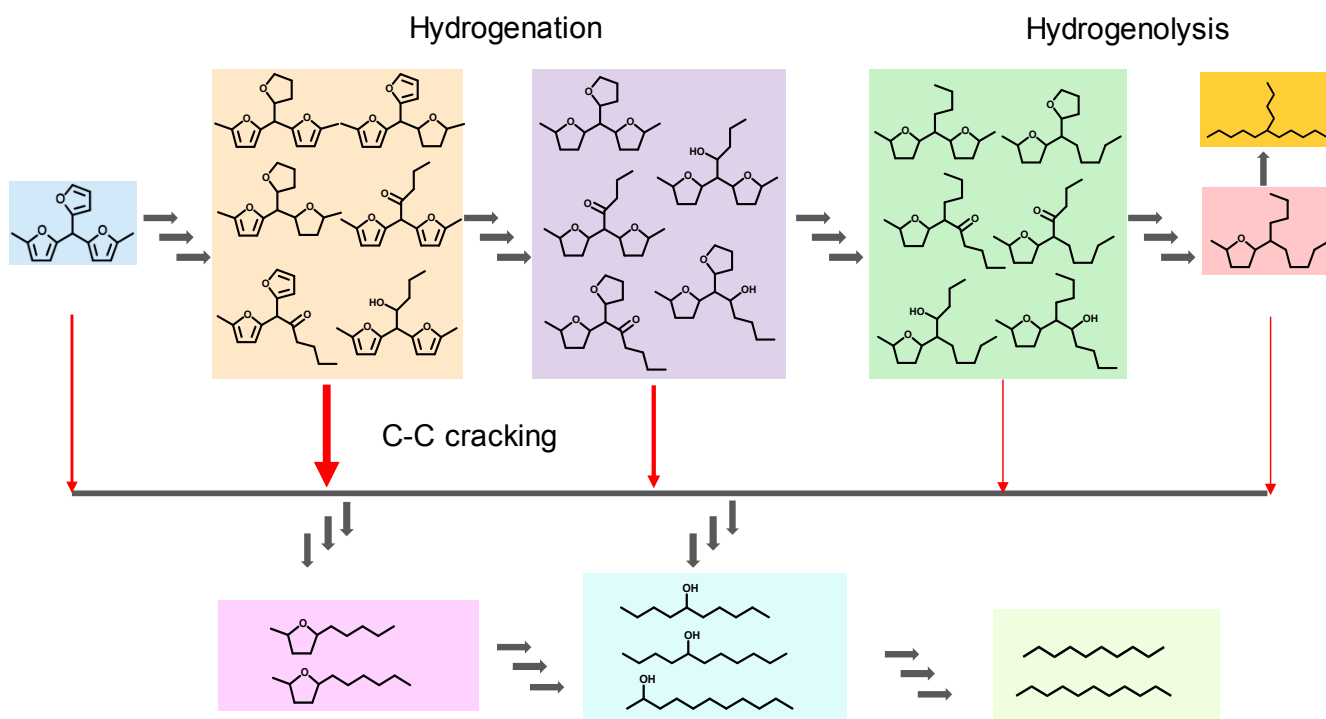
Scheme 2. Proposed reaction pathway for the conversion of C$_{15}$-HCF1 to fuels.

3.3 Application of Ir-MoO$_x$/SiO$_2$ to the production of lubricant base oils

Next, the Ir-MoO$_x$/SiO$_2$ (0.13) catalyst was used for the HDO of high carbon furan compounds to synthesize C$_{20}$-C$_{50}$ alkanes suitable for lubricant base oils, which have higher value than fuels (Scheme 1). Under the best reaction conditions used for the conversion of C$_{15}$-HCF1, HDO of C$_{30}$-HCF produces C30-A having structural and property similarity (Scheme 1) to commercial synthetic base-oils (PAO4) and superior properties than regular mineral base-oils[29, 52]. A maximum 84% yield of C$_{30}$-A is obtained over Ir-MoO$_x$/SiO$_2$ (0.13) (Table 3, Entry 1). A small fraction (~12% yield) of C−C cracking products *n*-nonane and *n*-heneicosane is detected. These linear alkanes

14

could increase the pour point of the resulting base-oil and lower its specification quality. Reaction at lower temperature (170 °C) yields 89% C_{30}-A with less yield (6%) to *n*-nonane and *n*-heneicosane (Table 3, Entry 2). Under comparable conditions, HDO of C_{20}-HCF yields 93% C_{20}-A (Table 3, Entry 3), which has similar structure as the commercial synthetic PAO2 base oil. These yields are slightly higher than that obtained (86%) over Ir-ReO$_x$/SiO$_2$ (2)[29]. Therefore, the Ir-MoO$_x$/SiO$_2$ (0.13) catalyst is promising for the production of lubricant base oils.

Table 3. Production of lubricant base oils by HDO of C_{30}-HCF and C_{20}-HCF over the Ir-MoO$_x$/SiO$_2$ (0.13) catalyst.

Entry	Substrate	T / °C	Conv. %	Yield %			
				Target alkane	C-C cracked alkanes		
1	C_{30}-HCF	180	100	C_{30} 84	C_{21} 7.5		C_9 4.2
2	C_{30}-HCF	170	100	C_{30} 89	C_{21} 4.2		C_9 2.1
3	C_{20}-HCF	170	100	C_{20} 93	C_{11} 1.2		C_9 1.5

Reaction conditions: catalyst (0.15 g), substrate (0.3 g), cyclohexane (10 mL), initial H_2 (5 MPa), 20 h.

3.4 Catalyst characterization results

We characterized pre-reduced Ir-MoO$_x$/SiO$_2$ by XRD, TEM, CO chemisorption, XPS, in-situ XAS, and Py-FT-IR techniques to elucidate the relationship between the properties of the catalysts and their performance. Figure 2 shows XRD patterns of pre-reduced Ir-MoO$_x$/SiO$_2$ (0.05-0.5), Ir/SiO$_2$, and MoO$_x$/SiO$_2$. The signals assigned to Ir metal are observed in all of the Ir-catalysts while no peak for MoO$_x$ is present, indicating that Ir is in metallic state, and MoO$_x$ species are likely highly dispersed or amorphous. The peak intensity of Ir metal slightly decreases with increasing Mo/Ir atomic ratio, suggesting a decrease in average particle size of Ir metal likely caused by the increasing amount of Mo. TEM images (Figure 3) show the average particle size (Table 4) of Ir metal in all the Ir-MoO$_x$/SiO$_2$ catalysts is smaller (3.4-3.8 nm) than those of Ir/SiO$_2$ (4.0 nm), consistent with the XRD data.
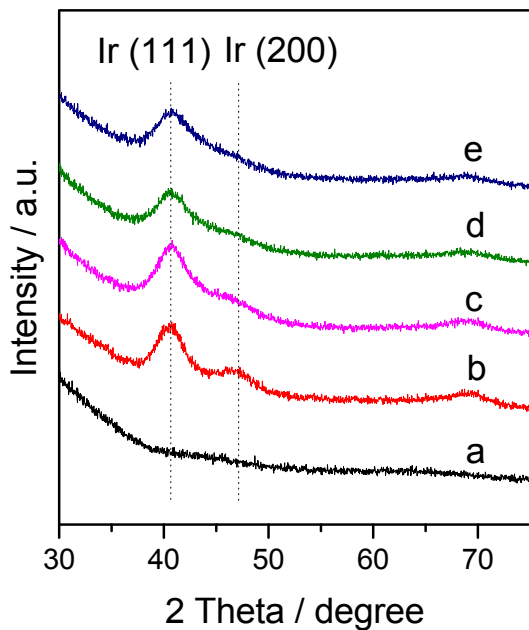
15

Figure 2. XRD patterns of the catalysts after reduction. a: MoO_x/SiO_2, b: Ir/SiO_2, c: $Ir\text{-}MoO_x/SiO_2$ (0.13), d: $Ir\text{-}MoO_x/SiO_2$ (0.25), e: $Ir\text{-}MoO_x/SiO_2$ (0.5)

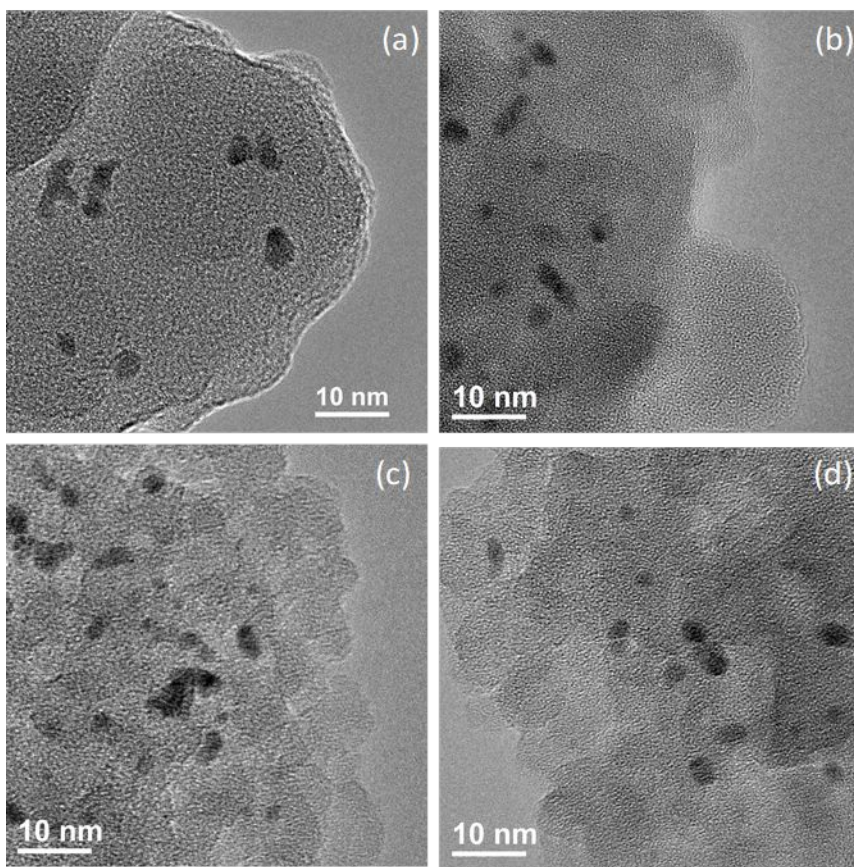**Figure 3.** TEM images of the pre-reduced catalysts. a: Ir/SiO_2, b: $Ir\text{-}MoO_x/SiO_2$ (0.13), c: $Ir\text{-}MoO_x/SiO_2$ (0.25), d: $Ir\text{-}MoO_x/SiO_2$ (0.5).

16

XPS profiles of pre-reduced Ir/SiO$_2$ and Ir-MoO$_x$/SiO$_2$ (0.13-0.5) in Ir 4f and Mo 3d regions are shown in Figure 4. Both Ir/SiO$_2$ and Ir-MoO$_x$/SiO$_2$ (0.13-0.5) samples show two peaks around 61 eV and 64 eV, which can be assigned to Ir^0 4f$_{7/2}$ and Ir^0 4f$_{5/2}$, respectively.[53] The result suggests that Ir is present in metallic state, consistent with the XRD analysis. The Mo 3d spectra show a peak shift of Mo species of pre-reduced Ir-MoO$_x$/SiO$_2$ (0.13-0.5) to a lower binding energy when compared with those of fresh Ir-MoO$_x$/SiO$_2$ obtained after calcination. The signals are mainly distributed between Mo^0 and Mo^{6+}, indicating partially reduced Mo species.

In situ XAS measurements at Mo k-edge were conducted to probe the bulk oxidation state of Mo species upon reduction in H$_2$ and compared with standards MoO$_3$, MoO$_2$, Mo foil and Na$_2$MoO$_4$ (Figure 5 and Figure S4). Prior to reduction, all catalysts (Ir-MoO$_x$/SiO$_2$ and MoO$_x$/SiO$_2$) showed the Mo 1s-4d pre-edge peaks at around 19997 eV [54], which are similar to those of MoO$_3$. Upon reducing in H$_2$ at 200 °C, the pre-edge peak of Ir-MoO$_x$/SiO$_2$ catalysts disappear and the edge energy of Mo shifts close to MoO$_2$. This result supports the XPS findings that Mo species are partially reduced at 200 °C in H$_2$. In contrast, the XANES spectra of MoO$_x$/SiO$_2$ without Ir remains constant in H$_2$ at 200 °C, while the reduction of supported MoO$_3$ clusters requires much higher temperature (>350 °C)[55]. These results indicate a strong interaction between Ir and MoO$_x$, where Ir significantly promotes the reduction of MoO$_x$ at mildly reducing condition, probably due to the H$_2$ spillover.
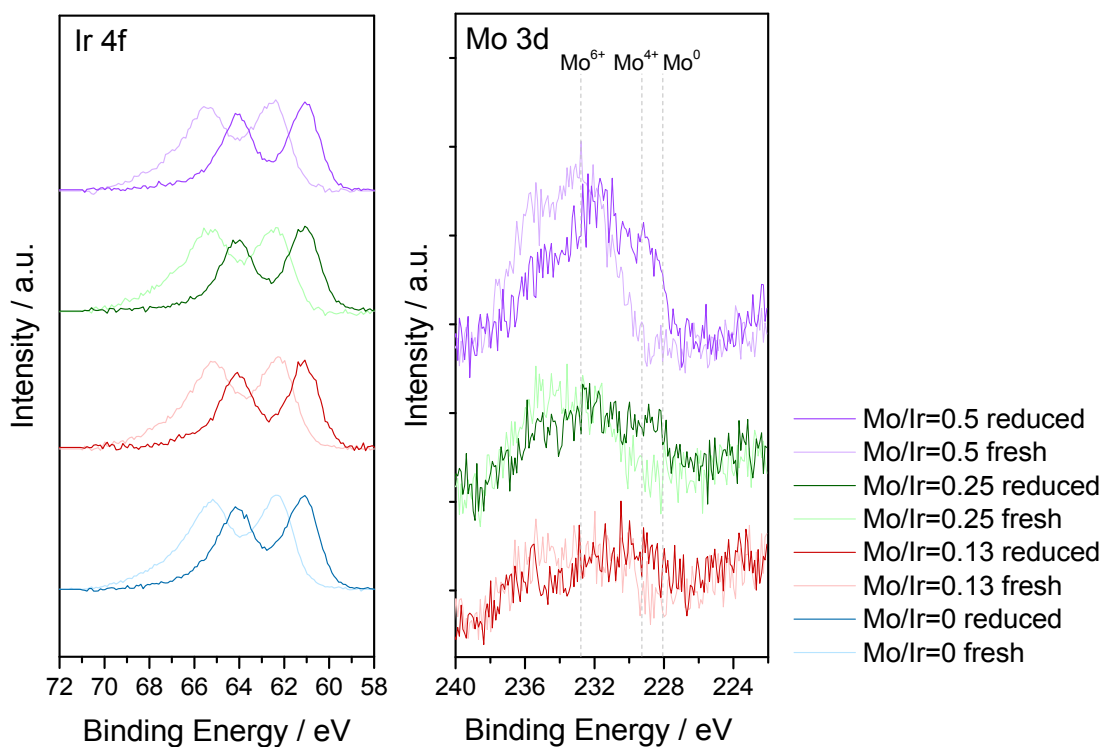
17

Figure 4. Normalized core-level Ir 4f and Mo 3d XPS spectra of Ir/SiO$_2$ and Ir-MoO$_x$/SiO$_2$ catalysts before reduction (fresh) and after reduction (reduced).
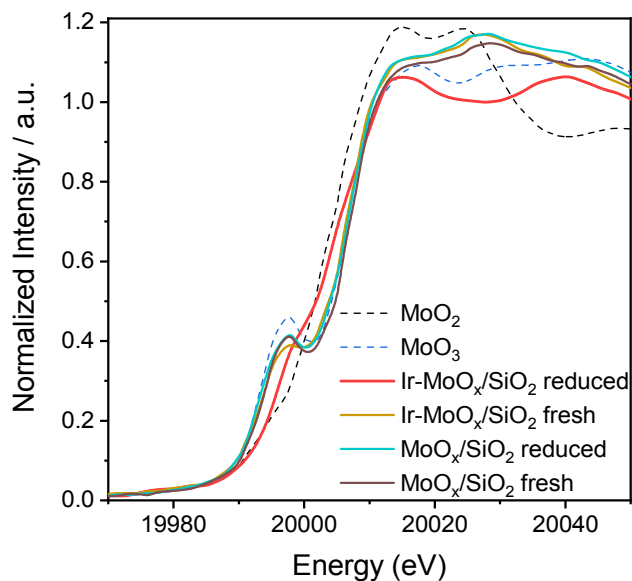

Figure 5. Mo K edge XANES spectra of Ir-MoO$_x$/SiO$_2$ (0.13) and MoO$_x$/SiO$_2$ before reduction (fresh) and after reduction (reduced) and corresponding standards (MoO$_2$ and MoO$_3$).

In order to determine the surface sites of Ir-MoO$_x$/SiO$_2$, CO chemisorption was conducted for Ir-MoO$_x$/SiO$_2$ (0.13-0.05), Ir/SiO$_2$, and MoO$_x$/SiO$_2$. The CO adsorption amount and the atomic ratio

18

of the surface Ir to the total Ir (CO/Ir) are shown in Table 3. The CO adsorption on the Ir metal sites of Ir/SiO$_2$ was calculated to be 0.041 mmol·g^{-1}, and the CO/Ir was estimated to be ~19.7%. The CO adsorption amount on Ir-MoO$_x$/SiO$_2$ (0.13-0.05) gradually decreases with increasing atomic ratio of Mo/Ir, suggesting less exposed Ir metal atoms, inconsistent with the decreasing particle size of Ir-MoO$_x$/SiO$_2$ (0.13-0.05). Given that MoO$_x$/SiO$_2$ does not adsorb CO, our hypothesis is that the Ir metal particle surface of Ir-MoO$_x$/SiO$_2$ is partially covered with MoO$_x$ species as suggested in other oxophilic metal oxides modified with noble metal catalysts, such as Ir-ReO$_x$/SiO$_2$ [56], Rh-ReO$_x$/SiO$_2$ [41], Rh-MoO$_x$/SiO$_2$ [38] and Pt-MoO$_x$/C [35].

Table 4. Summary of characterization results.

| Entry | Catalyst | CO chemisorption | | TEM |
		CO amount / mmol g^{-1}	CO/Ir ratio[a] / %	d^b / nm
1	Ir/SiO$_2$	0.041	19.7	4.0
2	Ir-MoO$_x$/SiO$_2$ (0.13)	0.037	17.8	3.8
3	Ir-MoO$_x$/SiO$_2$ (0.25)	0.022	10.5	3.4
4	Ir-MoO$_x$/SiO$_2$ (0.5)	0.019	9.2	3.5
5	MoO$_x$/SiO$_2$	0	-	-

a: Atomic ratio of the Ir on the surface to the total Ir, assuming the molar ratio of CO to surface Ir is equal to 1. b: The average particle size of Ir

Transmission FTIR spectroscopy of pyridine adsorbed on the *in-situ* reduced catalysts (Ir/SiO$_2$, MoO$_x$/SiO$_2$ and Ir-MoO$_x$/SiO$_2$ (0.13)) was used to evaluate their acidic properties. An IR band at 1450 cm^{-1} is assigned to pyridine adsorbed on Lewis acid sites (Figure S5), whereas a band at 1540 cm^{-1} emerges from pyridine interacting with Brønsted acidic sites[57]. In our earlier work, almost no adsorbed pyridine was observed on Ir/SiO$_2$ above 100 °C. In contrast, a band at ~1450 cm^{-1} was observed on both Ir-MoO$_x$/SiO$_2$ and MoO$_x$/SiO$_2$ at 150 °C, indicating the presence of Lewis acid sites from the partially reduced MoO$_x$ species. A peak corresponding to the Brønsted acid sites is also observed on Ir-MoO$_x$/SiO$_2$, consistent with our prior observation on Ir-ReO$_x$/SiO$_2$[16].
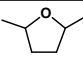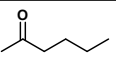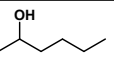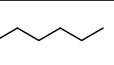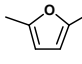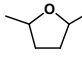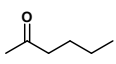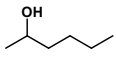
3.5 Ir-MoO$_x$ synergy revealed using probe-molecule chemistry

To understand the role of MoO$_x$ in the Ir-MoO$_x$/SiO$_2$ catalysts, hydrogenation and HDO of model compounds, such as DMF, DMTHF, 2-hexanone and 2-hexanol, were conducted at 120 °C. The turnover frequencies (TOFs) and product distribution over Ir/SiO$_2$ and Ir-MoO$_x$/SiO$_2$ (0.13)

19

are shown in Table 5. Both saturated furan ring (DMTHF) and ring opening products (2-hexanone and 2-hexanol) form during DMF conversion, in line with intermediates observed at the beginning of HDO of C_{15}-HCF1. This is consistent with prior reports[16, 58] that furan ring-opening of DMF to 2-hexanone and 2-hexanol and ring-saturation to DMTHF occur in parallel (Scheme 3). The reaction rate for hydrogenation of DMF over both catalysts is similar, suggesting the hydrogenation of furan rings mainly occurs over Ir sites (Table 5, Entry 1). This finding is consistent with the emerging picture is that most metals adsorb furans strongly in a flat conformation and carry out ring hydrogenation and ring opening. Bell and co-workers proposed that the interaction between the furan rings of the substrates and the metal surface is crucial in weakening the C-O bond of the furan rings, resulting in cleavage of the C-O bond.[59] DFT calculations and microkinetic modeling on the hydrogenation of DMF over Ru/C indicated that DMF absorbs on Ru in a flat configuration, which is potentially a common surface intermediate that leads to both ring-opening and ring-saturation products[58]. Although the activation barriers for the two pathways are comparable, formation of DMTHF is more thermodynamically favorable[58]. These are consistent with our finding that the selectivity to ring-saturation-product, DMTHF, is much higher than that to ring-opening-products, 2-hexanone and 2-hexanol. HDO of DMTHF to n-hexane over Ir-MoO$_x$/SiO$_2$ is more selectivity than over Ir/SiO$_2$ (Table 5, Entry 2). The reaction rates for the ring-opening of DMTHF and HDO of 2-hexanol over Ir-MoO$_x$/SiO$_2$ are ~2 and ~6 fold higher than those over Ir/SiO$_2$, respectively (Table 5, Entries 2 and 4). This finding suggests that MoO$_x$ in Ir-MoO$_x$/SiO$_2$ promotes ring opening of DMTHF as well as enhances the C−O hydrogenolysis of alcoholic groups. This finding could be due to the oxophilicity of MoO$_x$ and the acidic sites of Ir-MoO$_x$/SiO$_2$, which facilitate surface adsorption of the cyclic ether rings of DMTHF via its electronegative oxygen atoms and dehydration of alcohol (2-hexanol), derived from ring opening. Prior studies suggest that the acid sites on the partially reduced oxophilic metal oxides (e.g., ReO$_x$ and NbO$_x$) are critical for C−O hydrogenolysis of cyclic ethers and alcohols[47, 60]. Control experiments using 2-hexanone hydrogenation to 2-hexanol indicate that the rate over the Ir-MoO$_x$/SiO$_2$ catalyst is ~65 times higher than that over Ir/SiO$_2$ (Table 5, Entry 3). Thus, MoO$_x$ sites enhance C=O hydrogenation over metallic Ir. We attribute this enhanced rate to an interaction between the Lewis acidic sites on the partially reduced MoO$_x$ and the oxygen atom of the carbonyl group. Such interactions between partially reduced metals of NbO$_x$ and ReO$_x$ and the carbonyl group of unsaturated aldehydes have been demonstrated by *in situ* FTIR studies[43-44]. The

20

adjacent Ir metal dissociates hydrogen and spills this over for hydrogenation of ketone to an alcohol. Given the superior C−O hydrogenolysis and C=O hydrogenation activities of Ir-MoO$_x$/SiO$_2$, it is rational to apply this catalyst for the HDO of fatty acids, fatty esters and lipids to produce diesel-ranged alkanes (see examples for stearic acid, methyl stearate, palm oil, and soybean oil in Figure S6). Nearly quantitative yields of C$_9$-C$_{18}$ alkanes can be obtained.

Table 5. Conversion of different model compounds over Ir-MoO$_x$/SiO$_2$ (0.13) catalyst.

Entry	Substrate	Catalyst	Conv. /%	Selectivity / %				TOF[1] / h^{-1}
				(THF)	(ketone)	(OH)	(alkane)	
1	DMF	Ir/SiO$_2$	9.4	48.7	38.7	12.5	0.2	13796
		Ir-MoO$_x$/SiO$_2$	8.4	58.8	11.2	28.0	2.0	13401
2	DMTHF	Ir/SiO$_2$	1.5	-	-	24.7	75.3	18
		Ir-MoO$_x$/SiO$_2$	3.0	-	-	2.5	97.5	41
3	2-Hexanone	Ir/SiO$_2$	0.4	-	-	100	0	1209
		Ir-MoO$_x$/SiO$_2$	26	-	-	97.3	2.7	79428
4	2-Hexanol	Ir/SiO$_2$	0.6	-	-	-	100	37
		Ir-MoO$_x$/SiO$_2$	8.8	-	-	-	100	227

Reaction condition: catalyst (0.01-0.1g), substrate (1 g), cyclohexane (10 ml), initial N$_2$ (0.3 MPa at R. T.), N$_2$+H$_2$ (6MPa at 120 °C), 120 °C, 5 min-2 h. [1]: TOF were calculated based on the exposed Ir metal.
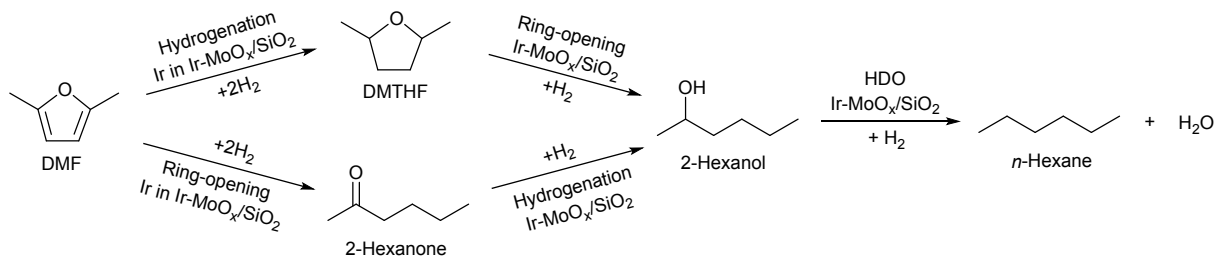
Scheme 3. Proposed reaction pathway for the conversion of DMF to *n*-hexane over the Ir-MoO$_x$/SiO$_2$ catalyst.

21

3.6 Catalyst reusability

Catalyst reusability is key for potential use of a catalytic process. We found the Ir-MoO$_x$/SiO$_2$ (0.13) catalyst is stable for the HDO of C$_{30}$-HCF; only 2% loss in the yield of C$_{30}$-A is observed after five consecutive runs (Figure 6). ICP-MS, XRD and TEM characterizations for both the fresh and used catalysts elucidate a slight deactivation of the catalyst. ICP-MS analysis of the reaction solution, after filtering off the catalyst, shows a negligible amount of Ir (0.0045 wt%, based on total Ir amount) and very slight leaching of Mo (0.2062 wt%, based on the total Mo amount).The XRD patterns of Ir-MoO$_x$/SiO$_2$ (0.13) after the 5th cycle show that the peaks assigned to Ir metal became sharper (Figure S7). The TEM images (Figure S8) show the particle size after the 5th cycle is 5.4 nm, which is larger than that of the fresh catalyst (3.8 nm), possibly due to sintering during reaction and/or recalcination. Therefore, 2% yield loss of C$_{30}$-A in the 5th cycle could be due to the combined effect of small amounts of metal leaching, especially Mo, and sintering of the catalyst.

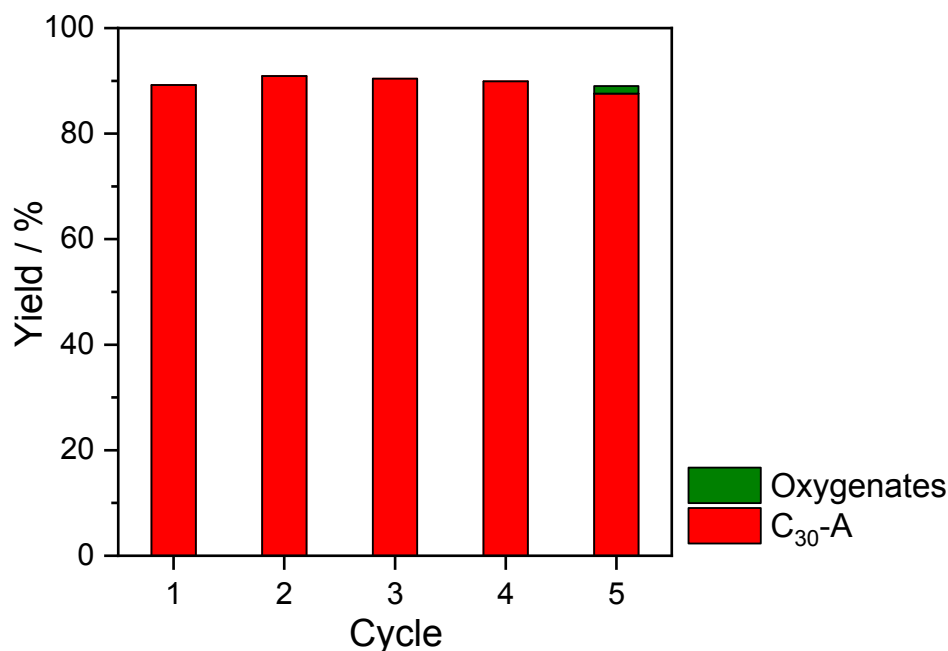**Figure 6.** Recyclability the Ir-MoO$_x$/SiO$_2$ (0.13) catalyst. Reaction conditions: catalyst (0.15 g), C$_{30}$-CF1 (0.3 g), cyclohexane (10 mL), initial H$_2$ (5 MPa), 170 ^{o}C, 20 h.

4. Conclusions

We have synthesized Ir-MO$_x$/SiO$_2$ (M=Re, Mo, W, V, or Nb) and M'-MoO$_x$/SiO$_2$ (M=Rh, Ru, Pt, or Pd) catalysts and screened them for the production of renewable fuel and lubricant base oils

22

from high carbon furan substrates under mild reaction conditions. MoO_x, WO_x, and VO_x oxophilic metal oxides improve the HDO activity of Ir/SiO_2, while NbO_x is ineffective. Among catalysts, MoO_x modified Ir/SiO_2 (Ir-MoO_x/SiO_2; Mo/Ir=0.13) is the most effective, and is superior to Ir-ReO_x/SiO_2 reported previously at low metal loading amount. High yields (78-96%) of fuels (C_8-C_{18}) and lubricant base oils (C_{20}-C_{50}) are achieved. Control experiments using HCFs with different functional groups suggest that the reaction progresses via hydrogenation and parallel ring opening of saturated and unsaturated furan rings to mono-keto and mono-hydroxy chains. These intermediates then undergo hydrogenolysis in a cascade sequence to alkanes. Modest C−C bond scission at the carbon atom adjacent to a furan or a saturated furan ring results in lower carbon alkanes. Detailed characterization of the Ir-MoO_x/SiO_2 catalyst suggests that MoO_x sites partially cover the Ir metallic particles and that the MoO_x sites facilitate ring opening, C−O hydrogenolysis of cyclic ethers and alcohols, and C=O hydrogenation. These results highlight the potential of low-cost oxophilic metal oxides modified noble metals and specifically of Ir-MoO_x/SiO_2 to enable cost-competitive production of bioproducts.

Acknowledgements

References

23

1. Huber, G. W.; Iborra, S.; Corma, A., Synthesis of Transportation Fuels from Biomass: Chemistry, Catalysts, and Engineering. *Chem. Rev.* **2006,** *106* (9), 4044-4098.

2. Bohre, A.; Dutta, S.; Saha, B.; Abu-Omar, M. M., Upgrading Furfurals to Drop-in Biofuels: An Overview. *ACS Sustainable Chem. Eng* **2015,** *3* (7), 1263-1277.

3. Deneyer, A.; Renders, T.; Van Aelst, J.; Van den Bosch, S.; Gabriëls, D.; Sels, B. F., Alkane production from biomass: chemo-, bio- and integrated catalytic approaches. *Curr. Opin. Chem. Biol.* **2015,** *29*, 40-48.

4. Han, X.; Guo, Y.; Liu, X.; Xia, Q.; Wang, Y., Catalytic conversion of lignocellulosic biomass into hydrocarbons: A mini review. *Catal. Today* **2019,** *319*, 2-13.

5. Nakagawa, Y.; Liu, S.; Tamura, M.; Tomishige, K., Catalytic Total Hydrodeoxygenation of Biomass-Derived Polyfunctionalized Substrates to Alkanes. *Chemsuschem* **2015,** *8* (7), 1114-1132.

6. Serrano-Ruiz, J. C.; Dumesic, J. A., Catalytic routes for the conversion of biomass into liquid hydrocarbon transportation fuels. *Energ. Environ. Sci.* **2011,** *4* (1), 83-99.

7. Climent, M. J.; Corma, A.; Iborra, S., Conversion of biomass platform molecules into fuel additives and liquid hydrocarbon fuels. *Green Chem.* **2014,** *16* (2), 516-547.

8. Calemma, V.; Peratello, S.; Stroppa, F.; Giardino, R.; Perego, C., Hydrocracking and Hydroisomerization of Long-Chain n-Paraffins. Reactivity and Reaction Pathway for Base Oil Formation. *Ind. Eng. Chem. Res.* **2004,** *43* (4), 934-940.

9. Corma, A.; de la Torre, O.; Renz, M., Production of high quality diesel from cellulose and hemicellulose by the Sylvan process: catalysts and process variables. *Energ. Environ. Sci.* **2012,** *5* (4), 6328-6344.

10. Corma, A.; de la Torre, O.; Renz, M., High-Quality Diesel from Hexose- and Pentose-Derived Biomass Platform Molecules. *Chemsuschem* **2011,** *4* (11), 1574-1577.

11. Corma, A.; de la Torre, O.; Renz, M.; Villandier, N., Production of High-Quality Diesel from Biomass Waste Products. *Angew. Chem. Int. Ed.* **2011,** *50* (10), 2375-2378.

12. Li, G.; Li, N.; Li, S.; Wang, A.; Cong, Y.; Wang, X.; Zhang, T., Synthesis of renewable diesel with hydroxyacetone and 2-methyl-furan. *Chem. Commun.* **2013,** *49* (51), 5727-5729.

13. Li, G.; Li, N.; Wang, Z.; Li, C.; Wang, A.; Wang, X.; Cong, Y.; Zhang, T., Synthesis of High-Quality Diesel with Furfural and 2-Methylfuran from Hemicellulose. *Chemsuschem* **2012,** *5* (10), 1958-1966.

14. Li, G.; Li, N.; Yang, J.; Li, L.; Wang, A.; Wang, X.; Cong, Y.; Zhang, T., Synthesis of renewable diesel range alkanes by hydrodeoxygenation of furans over Ni/Hβ under mild conditions. *Green Chem.* **2014,** *16* (2), 594-599.

15. Li, S.; Li, N.; Li, G.; Li, L.; Wang, A.; Cong, Y.; Wang, X.; Zhang, T., Lignosulfonate-based acidic resin for the synthesis of renewable diesel and jet fuel range alkanes with 2-methylfuran and furfural. *Green Chem.* **2015,** *17* (6), 3644-3652.

16. Liu, S.; Dutta, S.; Zheng, W.; Gould, N. S.; Cheng, Z.; Xu, B.; Saha, B.; Vlachos, D. G., Catalytic Hydrodeoxygenation of High Carbon Furylmethanes to Renewable Jet-fuel Ranged Alkanes over a Rhenium-Modified Iridium Catalyst. *Chemsuschem* **2017,** *10* (16), 3225-3234.

17. Xia, Q.; Xia, Y.; Xi, J.; Liu, X.; Zhang, Y.; Guo, Y.; Wang, Y., Selective One-Pot Production of High-Grade Diesel-Range Alkanes from Furfural and 2-Methylfuran over Pd/NbOPO4. *Chemsuschem* **2017,** *10* (4), 747-753.

18. Arias, K. S.; Climent, M. J.; Corma, A.; Iborra, S., Synthesis of high quality alkyl naphthenic kerosene by reacting an oil refinery with a biomass refinery stream. *Energ. Environ. Sci.* **2015,** *8* (1), 317-331.

19. Jing, Y.; Xia, Q.; Xie, J.; Liu, X.; Guo, Y.; Zou, J.-j.; Wang, Y., Robinson Annulation-Directed Synthesis of Jet-Fuel-Ranged Alkylcyclohexanes from Biomass-Derived Chemicals. *ACS Catal.* **2018,** *8* (4), 3280-3285.

20. Sutton, A. D.; Waldie, F. D.; Wu, R.; Schlaf, M.; 'Pete' Silks Iii, L. A.; Gordon, J. C., The hydrodeoxygenation of bioderived furans into alkanes. *Nat. Chem.* **2013,** *5*, 428.

24

21. Wang, L.; Chen, E. Y. X., Recyclable Supported Carbene Catalysts for High-Yielding Self-Condensation of Furaldehydes into C10 and C12 Furoins. *ACS Catal.* **2015,** *5* (11), 6907-6917.

22. Xia, Q.-N.; Cuan, Q.; Liu, X.-H.; Gong, X.-Q.; Lu, G.-Z.; Wang, Y.-Q., Pd/NbOPO4 Multifunctional Catalyst for the Direct Production of Liquid Alkanes from Aldol Adducts of Furans. *Angew. Chem. Int. Ed.* **2014,** *53* (37), 9755-9760.

23. Yang, J.; Li, N.; Li, S.; Wang, W.; Li, L.; Wang, A.; Wang, X.; Cong, Y.; Zhang, T., Synthesis of diesel and jet fuel range alkanes with furfural and ketones from lignocellulose under solvent free conditions. *Green Chem.* **2014,** *16* (12), 4879-4884.

24. Yang, J.; Li, S.; Zhang, L.; Liu, X.; Wang, J.; Pan, X.; Li, N.; Wang, A.; Cong, Y.; Wang, X.; Zhang, T., Hydrodeoxygenation of furans over Pd-FeOx/SiO2 catalyst under atmospheric pressure. *Appl. Catal. B: Environ.* **2017,** *201*, 266-277.

25. Wegenhart, B. L.; Yang, L.; Kwan, S. C.; Harris, R.; Kenttämaa, H. I.; Abu-Omar, M. M., From Furfural to Fuel: Synthesis of Furoins by Organocatalysis and their Hydrodeoxygenation by Cascade Catalysis. *Chemsuschem* **2014,** *7* (9), 2742-2747.

26. Balakrishnan, M.; Arab, G. E.; Kunbargi, O. B.; Gokhale, A. A.; Grippo, A. M.; Toste, F. D.; Bell, A. T., Production of renewable lubricants via self-condensation of methyl ketones. *Green Chem.* **2016,** *18* (12), 3577-3581.

27. Balakrishnan, M.; Sacia, E. R.; Sreekumar, S.; Gunbas, G.; Gokhale, A. A.; Scown, C. D.; Toste, F. D.; Bell, A. T., Novel pathways for fuels and lubricants from biomass optimized using life-cycle greenhouse gas assessment. *Proc. Natl. Acad. Sci.* **2015,** *112* (25), 7645-7649.

28. Gu, M.; Xia, Q.; Liu, X.; Guo, Y.; Wang, Y., Synthesis of Renewable Lubricant Alkanes from Biomass-Derived Platform Chemicals. *Chemsuschem* **2017,** *10* (20), 4102-4108.

29. Liu, S.; Josephson, T. R.; Athaley, A.; Chen, Q. P.; Norton, A.; Ierapetritou, M.; Siepmann, J. I.; Saha, B.; Vlachos, D. G., Renewable lubricants with tailored molecular architecture. *Science Advances* **2019,** *5* (2), eaav5487.

30. Dutta, S.; Bohre, A.; Zheng, W.; Jenness, G. R.; Núñez, M.; Saha, B.; Vlachos, D. G., Solventless C–C Coupling of Low Carbon Furanics to High Carbon Fuel Precursors Using an Improved Graphene Oxide Carbocatalyst. *ACS Catal.* **2017,** *7* (6), 3905-3915.

31. Liu, S.; Saha, B.; Vlachos, D., Catalytic Production of Renewable Lubricant Base-Oils from Bio-Based 2-Alkylfurans and Enals. *Green Chem.* **2019**.

32. https://apps.catalysts.basf.com/apps/eibprices/mp/defaultmain.aspx.

33. https://www.lme.com/Metals/Minor-metals/Molybdenum-Platts#tabIndex=0.

34. Tomishige, K.; Nakagawa, Y.; Tamura, M., Selective hydrogenolysis and hydrogenation using metal catalysts directly modified with metal oxide species. *Green Chem.* **2017,** *19* (13), 2876-2924.

35. Alba-Rubio, A. C.; Sener, C.; Hakim, S. H.; Gostanian, T. M.; Dumesic, J. A., Synthesis of Supported RhMo and PtMo Bimetallic Catalysts by Controlled Surface Reactions. *ChemCatChem* **2015,** *7* (23), 3881-3886.

36. Hakim, S. H.; Sener, C.; Alba-Rubio, A. C.; Gostanian, T. M.; O'Neill, B. J.; Ribeiro, F. H.; Miller, J. T.; Dumesic, J. A., Synthesis of supported bimetallic nanoparticles with controlled size and composition distributions for active site elucidation. *J. Catal.* **2015,** *328*, 75-90.

37. Koso, S.; Ueda, N.; Shinmi, Y.; Okumura, K.; Kizuka, T.; Tomishige, K., Promoting effect of Mo on the hydrogenolysis of tetrahydrofurfuryl alcohol to 1,5-pentanediol over Rh/SiO2. *J. Catal.* **2009,** *267* (1), 89-92.

38. Koso, S.; Watanabe, H.; Okumura, K.; Nakagawa, Y.; Tomishige, K., Comparative study of Rh–MoOx and Rh–ReOx supported on SiO2 for the hydrogenolysis of ethers and polyols. *Appl. Catal. B: Environ.* **2012,** *111-112*, 27-37.

39. Pholjaroen, B.; Li, N.; Huang, Y.; Li, L.; Wang, A.; Zhang, T., Selective hydrogenolysis of tetrahydrofurfuryl alcohol to 1,5-pentanediol over vanadium modified Ir/SiO2 catalyst. *Catal. Today* **2015,** *245*, 93-99.

25

40. Wang, Z.; Pholjaroen, B.; Li, M.; Dong, W.; Li, N.; Wang, A.; Wang, X.; Cong, Y.; Zhang, T., Chemoselective hydrogenolysis of tetrahydrofurfuryl alcohol to 1,5-pentanediol over Ir-MoOx/SiO2 catalyst. *Journal of Energy Chemistry* **2014,** *23* (4), 427-434.

41. Shinmi, Y.; Koso, S.; Kubota, T.; Nakagawa, Y.; Tomishige, K., Modification of Rh/SiO2 catalyst for the hydrogenolysis of glycerol in water. *Appl. Catal. B: Environ.* **2010,** *94* (3), 318-326.

42. Arai, T.; Tamura, M.; Nakagawa, Y.; Tomishige, K., Synthesis of 2-Butanol by Selective Hydrogenolysis of 1,4-Anhydroerythritol over Molybdenum Oxide-Modified Rhodium-Supported Silica. *Chemsuschem* **2016,** *9* (13), 1680-1688.

43. Tamura, M.; Tokonami, K.; Nakagawa, Y.; Tomishige, K., Selective Hydrogenation of Crotonaldehyde to Crotyl Alcohol over Metal Oxide Modified Ir Catalysts and Mechanistic Insight. *ACS Catal.* **2016,** *6* (6), 3600-3609.

44. Tamura, M.; Tokonami, K.; Nakagawa, Y.; Tomishige, K., Effective NbOx-Modified Ir/SiO2 Catalyst for Selective Gas-Phase Hydrogenation of Crotonaldehyde to Crotyl Alcohol. *ACS Sustainable Chem. Eng* **2017,** *5* (5), 3685-3697.

45. Tamura, M.; Tamura, R.; Takeda, Y.; Nakagawa, Y.; Tomishige, K., Catalytic hydrogenation of amino acids to amino alcohols with complete retention of configuration. *Chem. Commun.* **2014,** *50* (50), 6656-6659.

46. Tamura, M.; Tamura, R.; Takeda, Y.; Nakagawa, Y.; Tomishige, K., Insight into the Mechanism of Hydrogenation of Amino Acids to Amino Alcohols Catalyzed by a Heterogeneous MoOx-Modified Rh Catalyst. *Chem.-Eur. J.* **2015,** *21* (7), 3097-3107.

47. Xue, F.; Ma, D.; Tong, T.; Liu, X.; Hu, Y.; Guo, Y.; Wang, Y., Contribution of Different NbOx Species in the Hydrodeoxygenation of 2,5-Dimethyltetrahydrofuran to Hexane. *ACS Sustainable Chem. Eng* **2018,** *6* (10), 13107-13113.

48. West, R. M.; Tucker, M. H.; Braden, D. J.; Dumesic, J. A., Production of alkanes from biomass derived carbohydrates on bi-functional catalysts employing niobium-based supports. *Catal. Commun.* **2009,** *10* (13), 1743-1746.

49. West, R. M.; Liu, Z. Y.; Peter, M.; Dumesic, J. A., Liquid Alkanes with Targeted Molecular Weights from Biomass-Derived Carbohydrates. *Chemsuschem* **2008,** *1* (5), 417-424.

50. Shao, Y.; Xia, Q.; Liu, X.; Lu, G.; Wang, Y., Pd/Nb2O5/SiO2 Catalyst for the Direct Hydrodeoxygenation of Biomass-Related Compounds to Liquid Alkanes under Mild Conditions. *Chemsuschem* **2015,** *8* (10), 1761-1767.

51. Kon, K.; Onodera, W.; Takakusagi, S.; Shimizu, K.-i., Hydrodeoxygenation of fatty acids and triglycerides by Pt-loaded Nb2O5 catalysts. *Catal. Sci. Technol.* **2014,** *4* (10), 3705-3712.

52. Ray, S.; Rao, P. V. C.; Choudary, N. V., Poly-α-olefin-based synthetic lubricants: a short review on various synthetic routes. *Lubr. Sci.* **2012,** *24* (1), 23-44.

53. Keels, J. M.; Chen, X.; Karakalos, S.; Liang, C.; Monnier, J. R.; Regalbuto, J. R., Aqueous-Phase Hydrogenation of Succinic Acid Using Bimetallic Ir–Re/C Catalysts Prepared by Strong Electrostatic Adsorption. *ACS Catal.* **2018,** *8* (7), 6486-6494.

54. Ressler, T.; Timpe, O.; Neisius, T.; Find, J.; Mestl, G.; Dieterle, M.; Schlögl, R., Time-Resolved XAS Investigation of the Reduction/Oxidation of MoO3−x. *J. Catal.* **2000,** *191* (1), 75-85.

55. Fu, J.; Vasiliadou, E. S.; Goulas, K. A.; Saha, B.; Vlachos, D. G., Selective hydrodeoxygenation of tartaric acid to succinic acid. *Catal. Sci. Technol.* **2017,** *7* (21), 4944-4954.

56. Amada, Y.; Shinmi, Y.; Koso, S.; Kubota, T.; Nakagawa, Y.; Tomishige, K., Reaction mechanism of the glycerol hydrogenolysis to 1,3-propanediol over Ir–ReOx/SiO2 catalyst. *Appl. Catal. B: Environ.* **2011,** *105* (1), 117-127.

57. Busch, O. M.; Brijoux, W.; Thomson, S.; Schüth, F., Spatially resolving infrared spectroscopy for parallelized characterization of acid sites of catalysts via pyridine sorption: Possibilities and limitations. *J. Catal.* **2004,** *222* (1), 174-179.

58. Gilkey, M. J.; Mironenko, A. V.; Yang, L.; Vlachos, D. G.; Xu, B., Insights into the Ring-Opening of Biomass-Derived Furanics over Carbon-Supported Ruthenium. *Chemsuschem* **2016,** *9* (21), 3113-3121.

26

59. Louie, Y. L.; Tang, J.; Hell, A. M. L.; Bell, A. T., Kinetics of hydrogenation and hydrogenolysis of 2,5-dimethylfuran over noble metals catalysts under mild conditions. *Appl. Catal. B: Environ.* **2017,** *202,* 557-568.

60. Nakagawa, Y.; Mori, K.; Chen, K.; Amada, Y.; Tamura, M.; Tomishige, K., Hydrogenolysis of CO bond over Re-modified Ir catalyst in alkane solvent. *Appl. Catal. A: Gen.* **2013,** *468*, 418-425.

Table of Contents

27